Journal of Photochemistry and Photobiology A: Chemistry 349 (2017) 63–72

Contents lists available at ScienceDirect

Journal of Photochemistry and Photobiology A: Chemistry

journal homepage: www.elsevier.com/locate/jphotochem

A novel multilayered photoelectrode with nitrogen doped TiO_2 for efficiency enhancement in dye sensitized solar cells

M.A.K.L. Dissanayake[a,b,*], J.M.K.W. Kumari[a,b], G.K.R. Senadeera[a,b,c], C.A. Thotawatthage[a,b], B.-E. Mellander[d], I. Albinsson[e]

[a] National Institute of Fundamental Studies, Kandy, Sri Lanka
[b] Postgraduate Institute of Science, University of Peradeniya, Peradeniya, Sri Lanka
[c] Department of Physics, The Open University of Sri Lanka, Nawala, Nugegoda, Sri Lanka
[d] Department of Applied Physics, Chalmers University of Technology, Gothenburg, Sweden
[e] Department of Physics, University of Gothenburg, Gothenburg, Sweden

ARTICLE INFO

Article history:
Received 22 May 2017
Received in revised form 14 August 2017
Accepted 20 August 2017
Available online 8 September 2017

Keywords:
TiO_2 multilayer photoelectrode
N-doped TiO_2
Dye sensitized solar cells
Efficiency enhancement

ABSTRACT

Nitrogen doped TiO_2 powder samples were synthesized by a modified wet chemical method using aqueous ammonia and nitrogen gas purged on titanium tetra isopropoxide (TTIP). Photolectrodes with different combinations of layers of nitrogen – doped TiO_2, undoped TiO_2 and Degussa P25 TiO_2 powders were used in dye sensitized solar cells (DSSCs). The highest conversion efficiency of 8.00% was achieved by the cells fabricated with compact layer/P25/N-doped TiO_2 multilayer photoelectrode. This is an impressive enhancement in efficiency close to 89% with respect to a similar multilayer electrode made with undoped TiO_2 which showed a conversion efficiency of 4.22%. The enhancement in the efficiency appears to be due to the increased photocurrent density of the DSSCs resulting mainly from energy band gap narrowing due to N-doping with some contribution from increased dye uptake by the novel multilayer electrode. These results have been substantiated by the reduced charge transfer resistance obtained from Electrochemical Impedance Spectra and the enhanced IPCE spectra of the DSSCs with N-doped TiO_2 based multilayer electrode.

1. Introduction

Dye sensitized solar cells (DSSCs) [1,2] have been attracting much attention because of their relatively high energy conversion efficiency, low manufacturing cost, non-toxicity and simple fabrication process. Since the introduction of the DSSCs by Grätzel and co-workers in 1991, many improvements have been achieved towards enhancing the overall efficiencies of these devices. These includes the introduction of new dyes [3,4], new electrolytes [5,6] and different nano-structural modifications and morphologies to the semiconductor photoanode materials [7–9]. However, further improvements in the efficiency and stability are needed before these DSSCs are developed to commercial scale manufacturing.

At the heart of the DSSC system is a wide band gap oxide semiconductor such as TiO_2, which is placed in contact with a redox electrolyte. These semiconductor oxide films adsorb dye molecules and transport photo generated electrons to the outer circuit. Nano-crystalline mesoporous photo-anodes made of TiO_2 as one of the most widely used semiconductors show excellent performance in the DSSCs. Due to low cost, abundance in the world market, nontoxicity and biocompatibility, nano-size TiO_2 has become the best choice among semiconductors for DSSC applications as photoanodes. Other semiconducting materials such as ZnO [10], SnO_2 [11], Nb_2O_5 [12] etc have also been studied as possible photo-anode materials for DSSCs. However, the photovoltaic performance of DSSCs based on these semiconductor materials remains low and still cannot compete with TiO_2. In recent years a significant progress have been made on the improvement of overall conversion efficiencies of DSSCs by several groups including ours, by doping TiO_2 with materials such as metals (Zn, Nb, Au, Ag etc.) [13–16] and non- metals (N, B, C etc.) [17–19]. Recently, DSSCs based on liquid electrolytes with cobalt redox couple have exceeded 12% efficiency which is the highest reported efficiency for DSSCs up to now [20].

In this paper we report a novel multilayer photoelectrode with configuration, compact layer/P25/N-doped TiO_2 consisting of nitrogen doped TiO_2 layer, which can enhance the overall energy conversion efficiency of DSSC significantly.

* Corresponding author at: National Institute of Fundamental Studies, Kandy, Sri Lanka.
E-mail address: makldis@yahoo.com (M.A.K.L. Dissanayake).

http://dx.doi.org/10.1016/j.jphotochem.2017.08.067
1010-6030/

In case of nitrogen doping, various methods have been reported for the synthesis of N-doped TiO_2, since the study by Asahi et al. [17]. These methods can generally be classified as (a) sintering TiO_2 at high temperatures under a nitrogen containing atmosphere (ex. N_2 gas, NH_3 gas), which is known as the dry method [21], (b) Sol-gel and solvothermal methods known as wet chemical methods [22] and (c) Sputtering and implantation deposition techniques that have been mainly used to prepare single crystalline or polycrystalline N-doped TiO_2 thin films [23].

However, in previous studies researchers have used the conventional single layer concepts in fabrication of photoelectrodes in their devices. In this paper we report a novel multilayer photoelectrode concept with configuration, compact layer/P25/N-doped TiO_2 consisting of nitrogen doped TiO_2 layer, which can enhance the overall energy conversion efficiency of DSSCs significantly. For this purpose, here we used a slightly modified wet chemical method to synthesize the nanocrystalline N-doped TiO_2 using ammonia and N_2 gas as nitrogen dopant sources. For the resulting N-doped TiO_2 powder the structural characterization was done by XRD and optical characterization was done by UV–vis absorption spectroscopy. The surface morphologies and the thickness of the N-doped and P25 TiO_2 films were determined by scanning electron microscope (SEM). DSSCs with six different photoelectrode configurations consisting of different types of TiO_2 layers including N-doped TiO_2, undoped TiO_2 and P25 TiO_2 were fabricated and characterized using *J-V* measurements, IPCE measurements, charge transfer resistance and electron lifetime measurements.

2. Experimental

2.1. Materials

Titanium tetra isopropoxide (TTIP) and 35% purity aqueous ammonia were purchased from Fluka. Titanium dioxide powder (P25 TiO_2) was purchased from Degussa AG. Fluorine-doped conducting Tin Oxide (FTO) glass (Solaronix sheet glass 8 X/sq) and Ruthenium dye N 719 were purchased from Solaronix. Nitric acid (BDH) and Triton-X 100 (Aldrich) were used to prepare TiO_2 doctor-blade paste. Ethylene carbonate (EC) (Aldrich), tetrapropylammonium iodide (Pr_4NI) (98%, Aldrich), Acetonitrile (Aldrich) and iodine (Fluka) were used to prepare liquid electrolyte.

2.2. Synthesis of N-doped TiO_2 powder

N-doped TiO_2 powders were synthesized by slightly modified wet chemical method using hydrolysis of Titanium tetra isopropoxide (TTIP) with aqueous ammonia. The process is described as follows [21]. A 25 ml of titanium tetra isopropoxide was added drop wise to a 100 ml solution of deionized water and 50 ml of 35% aqueous ammonia (N/Ti molar ratio is 15) while purging N_2 gas. The hydrolysis was carried out under vigorous stirring in an ice bath. The white precipitate formed was washed with distilled deionized water several times. Precipitate was then dried at 80 °C for 1 h and it was subsequently sintered at 450 °C for 4 h and finally obtained a powder with yellowish colour. For comparison, undoped TiO_2 powder was also prepared without adding aqueous ammonia and purging with N_2 gas.

During the above preparation procedure, nitrogen doping proceeded simultaneously with the hydrolysis of the titanium tetra isopropoxide (TTIP). The hydrolysis of TTIP consisted of two steps, hydrolysis and concentration. In the hydrolysis step, acidic titanium hydroxide (titanic acid) is formed and then it reacts with NH_4OH to form ammonium titanate according to the reaction given by following equation [24].

$$H_2TiO_3.nH_2O + xNH_4OH \rightarrow (NH_4)_{xH2-x}TiO_3.nH_2O + x/2H_2O$$

When the resulting ammonium titanate is heated, it becomes dehydrated and with removal of NH_3, the N-doping occurs. This process can be summarized as follows:

$$(NH_4)_{xH2-x}TiO_3.nH_2O \rightarrow (NH_4)_{x-y}TiO_{2+1/2(x-y)} + yNH_3 + (n+2-x)\,H_2O$$

Ammonia in the doped samples becomes oxidized by the lattice oxygen, and this oxidation allows for the uptake of nitrogen. This can be represented as follows:

$$(NH_4)_{x-y}TiO_{2+1/2(x-y)} \rightarrow N_{x-y}TiO_{2-1/2(x-y)} + 2(x\text{-}y)\,H_2O$$

Here the ratio between Oxygen vacancies and amount of N dopant determine the photoelectrical properties of the N-doped TiO_2 material. Hence Ti/N molar ratio was taken as 15 by referring to the work reported by Wei Guo et al. [21] for the DSSCs with higher photovoltaic performance.

2.3. Preparation of multilayer photoelectrodes with P25, N-doped and undoped TiO_2 powder

Six different configurations of photoelectrodes were prepared with N-doped TiO_2, undoped TiO_2 and Degussa TiO_2 P25 powder. At first, compact layer solution was prepared by mixing 5.0 ml of Titanium tetra isopropoxide (TTIP), 5.0 ml of Propan-1-ol, 5.0 ml of acetic acid and 40.0 ml of ethanol. The solution was spin coated on to a pre-cleaned Fluorine doped conducting Tin Oxide (FTO) glass (Solaronix sheet glass 8 Ω/sq) and sintered at 450 °C for 30 min. The following method was used to prepare the paste for doctor blading. 0.25 g of N-doped TiO_2 powder and 0.1 M HNO_3 1.0 ml solution were mixed and ground using a mortar and pestle. 0.02 g of Triton X-100 and 0.05 g of PEG 1000 were added as the binder and the grinding continued until the mixture became a creamy paste. The paste was then doctor bladed on a FTO plate containing the compact layer while keeping the active cell area as 0.25 cm^2. For comparison purposes, electrodes with P25 and undoped TiO_2 were also prepared separately following the above procedure. All six photoelectrodes, (A) P25 TiO_2, (B) undoped TiO_2, (C) N-doped TiO_2, (D) compact layer/P25/P25, (E) compact layer/P25/undoped TiO_2 and (F) compact layer/P25/N-doped TiO_2 were prepared by doctor blade method and sintered at 450 °C for 45 min and slowly cooled down to room temperature.

2.4. Fabrication of DSSCs and I–V characterization

DSSCs with different types of TiO_2 electrodes were dipped in a dye solution of 3×10^{-4} M Ruthenium dye N719 [RuL2 (NCS)2: 2 TBA where, L = 2,2′-bipyridyl-4′, dicarboxylic acid; TBA = tetrabutyl ammonium] dissolved in ethanol, at 45 °C temperature for 15 h to obtain the dye-sensitized P25, undoped and N-doped TiO_2 photoelectrodes. The active cell area was 0.25 cm^2. These electrodes were assembled by sandwiching a redox (I^-/I_3^-) electrolyte solution between a dye-sensitized electrode and a platinized counter electrode. The redox electrolyte solution was prepared by dissolving 0.738 g tetrapropyl ammonium iodide (Pr_4NI) and 0.060 g of I_2 in 3.6 ml of molten (MP 40 °C) ethylene carbonate (EC) and 1.0 ml of acetonitrile. This solution mixture was stirred overnight and used to fabricate DSSCs.

2.5. DSSC characterization

The morphology of the TiO_2 and N-doped TiO_2 electrodes were observed by the Scanning Electron Microscope (HITACHI-SU8220).

The photocurrent-voltage (I–V) characteristics of the cells were measured under the illumination of 100 mW cm^{-2} (AM 1.5) simulated sunlight using a computer controlled setup coupled to a Keithley 2000 multimeter and a Potntiostat/galvanostat HA-301. A Xenon 500 W lamp was used with AM 1.5 filter to obtain the simulated sunlight with above intensity. Reproducibility of the I–V characteristic data was ensured by repeating I–V measurements at least for four solar cells prepared with identical photoelectrodes.

The incident photon-to-current conversion efficiency (IPCE) measurements were taken for all the above DSSCs fabricated with aforementioned six types of photoelectrodes. Experimental setup consisted of monochromatic light illumination from a Bentham PVE 300 unit with a TMC 300 monochromator based IPCE system with a 150 W Xenon arc lamp covering the 300 nm to 800 nm wavelength range. A calibrated Si photo detector (type DH) was used as the reference. Electrochemical Impedance Spectroscopy (EIS) measurements were performed on the DSSCs with different TiO_2 photoanodes using a Metrohm Autolab Potentiostat/galvanostat PGSTAT 128N with a FRA 32 M Frequency Response Analyzer (FRA) in the frequency range between 0.01 and 1×10^6 Hz. These measurements were carried out under the illumination of 100 mW cm^{-2} using the same solar simulator that was used for I–V measurements. The negative value of open circuit voltage (V_{oc}) of the DSSC was applied as the biased voltage to measure the impedance of the DSSC. Photovoltaic decay measurements were taken by the solar cell was set to open circuit state by setting the current in the Metrohm Autolab Potentiostat to zero. Then the cell was illuminated by low intensity white light. After the cell reached the steady state, it was exposed to red laser light. The laser light was then switched off and the resulting decay of the photovoltage with time was measured.

2.6. Characterization of the P25, undoped TiO_2 and N-doped TiO_2 powder

The phase composition and crystallinity of the P25, undoped and N-doped TiO_2 powders were determined using X-ray Diffraction analyzer (BTX compact Benchtop X-ray Diffraction System) with Cu Kα radiation (λ = 0.1541 nm). The crystal size was calculated by Scherrer's equation: $D = k\lambda/\beta\ Cos\theta$, where D represents the crystal size, k is the dimensionless shape factor with a typical value of 0.89, λ is the wavelength of the X-ray irradiation (0.1541 nm for Cu kα radiation), β is the full width at half of the maximum, and θ is Bragg's diffraction angle. At the same time, the phase composition was calculated from quantitative formula [25]:

$$x = (1 + 0.8\ I_A/I_R)^{-1},$$

where x is the weight fraction of rutile in the sample, I_A and I_R are the X-ray intensities of the anatase and rutile peaks, respectively.

The UV–vis absorption spectra of powder samples were taken by diffused reflection method. For these measurements, photoelectrodes were prepared from the paste of P25, undoped TiO_2 and N-doped TiO_2 on FTO glass plates as in the previous case and after sintering at 450 °C for 45 min the powders were scratched off from the glass plate and used to take the diffused reflection spectra using a Shimadzu 2450 UV–vis spectrophotometer in the wavelength range from 300 nm to 800 nm. Energy gap of each powder sample was calculated using the absorption spectrum.

The amount of dye loading of each phtoelectrode was calculated using UV–vis absorption spectrum. All phtoelectrodes were prepared with 0.25 cm^2 cell area. These electrodes were immersed in 1.0 ml of 0.3×10^{-3} mol dm^{-3} concentrated Ru N719 dye in ethanol, for 15 h. Photometric method was used to determine the absorbed dye amount. First, a calibration curve was obtained by using known concentrations of Ru dye solutions. The unknown concentrations of remaining dye solution after dipping the electrodes were calculated using this calibration curve. The amount of adsorbed dye by 0.25 cm^2 cell area from each electrodes were calculated by taking the difference between the initial concentration and the remaining dye concentration of the dye solutions in mol cm^{-2}.

3. Results and discussion

3.1. Morphology of N-doped TiO_2 photoelectrode

Fig. 1(a) shows a SEM image of a cross sectional view of the double layered photoelectrode with P25 and N-doped TiO_2. The lower part shows the P25 TiO_2 layer with the thickness of 9.13 μm and the upper part shows the N-doped TiO_2 layer with the thickness of 10.5 μm. Fig. 1(b) and (c) shows the top view of N-doped TiO_2 electrode and P25 TiO_2 electrode, respectively. These SEM images confirm that both samples consist of spherical TiO_2 particles and are to some extend agglomerated.

Energy Dispersive X-ray (EDX) analysis was also done for a selected area of N-doped TiO_2 electrode and normal TiO_2 electrode. Fig. 2(a) graph shows the EDX pattern for N-doped TiO_2 electrode and (b) shows the EDX graph for normal TiO_2 electrode. According to the EDX data, both electrodes contain Titanium, Oxygen and Carbon with different percentages. Especially in N-doped TiO_2, the presence of 5% of Nitrogen is observed. Atomic percentages of elements taken from EDX data are tabulated in Table 1.

3.2. XRD analysis

Undoped TiO_2 powder white in colour (left) and N-doped TiO_2 (right) powder yellowish in colour prepared in this work are shown in Fig. 3.

XRD measurements were used for the structural characterization of six different TiO_2 powder samples and the XRD spectra are shown in Fig. 4. Traces 1, 2 and 3 correspond to P25, undoped TiO_2 and N-doped TiO_2 after sintering at 450 °C for 4 h. Traces 4, 5 and 6 correspond to P25 powder, undoped TiO_2 powder and N-doped TiO_2 powder scratched off from FTO plates from doctor bladed samples using the paste made with HNO_3 acid. The X-ray structure analysis of the N-doped TiO_2 and undoped TiO_2 powder showed that the characteristic peaks of the anatase phase were observed but the peaks corresponding to the rutile phase were absent. Similar results were reported by several groups [18,25–28].

The polycrystalline anatase structure of sintered undoped and N-doped TiO_2 was further confirmed by (101), (103), (004), (112), (200) and (105) diffraction peaks [26]. Table 2 shows the percentages of anatase phase in the prepared TiO_2 powder samples extracted from XRD data. Degussa P25 TiO_2 powder was reported to be composed of 80.7% anatase and 19.3% rutile [29]. However, the undoped TiO_2 and N-doped TiO_2 powder samples composed only of the anatase phase. The rutile peaks of P25 powder samples were obtained at 2θ values, 27.45° (110), 36.10° (101) and 41.25° (111) [27].

Kim et al. have studied the effects of graphene in dye-sensitized solar cells based on nitrogen-doped TiO_2 composite [30] In their N-incorporated TiO_2 samples (without graphine) the presence of nitrogen after the calcination process at 500 °C for 2 h was confirmed by XPS measurements. Using XRD measurements, it was shown that the added amounts of nitrogen did not affect the TiO_2 crystalline structure but has contributed to make the particle size smaller which has enhanced the energy conversion efficiency of the solar cells significantly. The same group has reported the enhancement of efficiency in dye-sensitized solar cells fabricated

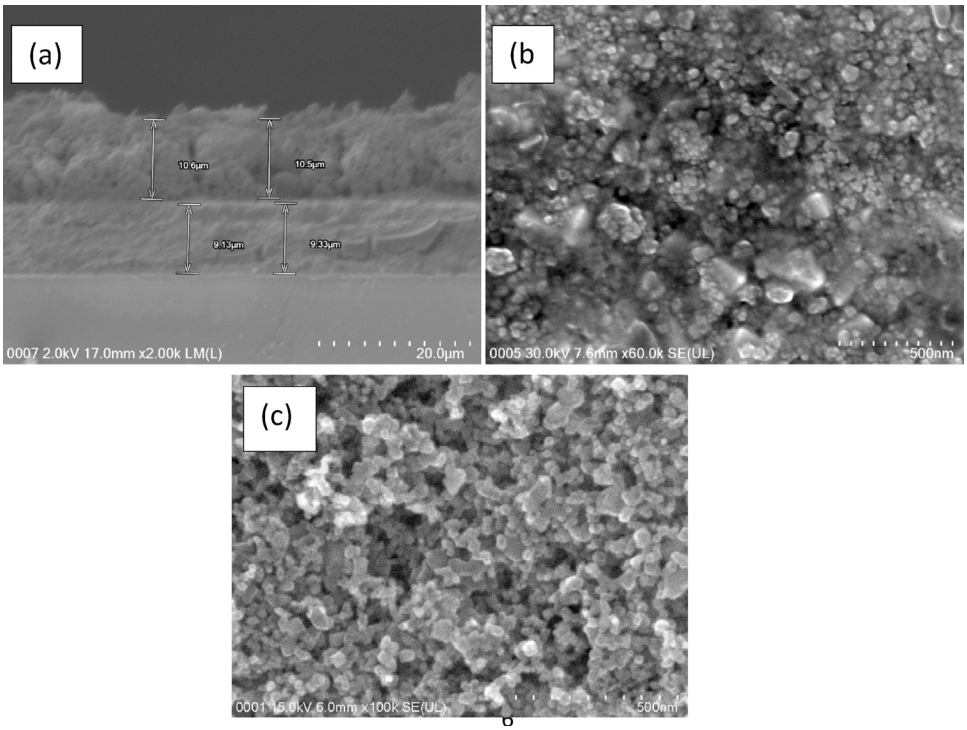

Fig. 1. SEM images of the (a) cross sectional view of the double layered photoelectrode with P25 and N-doped TiO_2, (b) top view of N-doped TiO_2 electrode film and (c) top view of P25 TiO_2 electrode film.

with Zr/N-doped TiO_2 photoelectrodes [31]. From their XRD measurements it was found that the P25 TiO_2 powder showed both the anatase and rutile phases but the N-doped TiO_2 nanoparticles showed only the anatase phase and that the insertion of Zr did not cause an anatase-to-rutile phase transformation. Similar to their earlier results, and based on XRD measurements, they have shown that the Degussa P25 nanoparticles exhibited anatase and rutile phases while the N-doped TiO_2 powder exhibited the anatase phase. The presence of N in N-TiO_2 was confirmed through XPS analysis.

This group has also reported the effect of Cu/N doped TiO_2 on efficiency enhancement in DSSCs[32]. From XPS measurements of normal undoped TiO_2 and Cu/N-doped TiO_2, it was shown that the undoped TiO_2 samples consisted of only three elements Ti, O, and C. However, the XPS spectra showed new peaks which matched with the binding energies of N 1s and Cu 2p, respectively. These results indicate that the Cu and N were dispersed onto the TiO_2 nanoparticles. N and Ti were determined at the same place and N was not quantitatively measured because of its lower concentration than Ti [32].

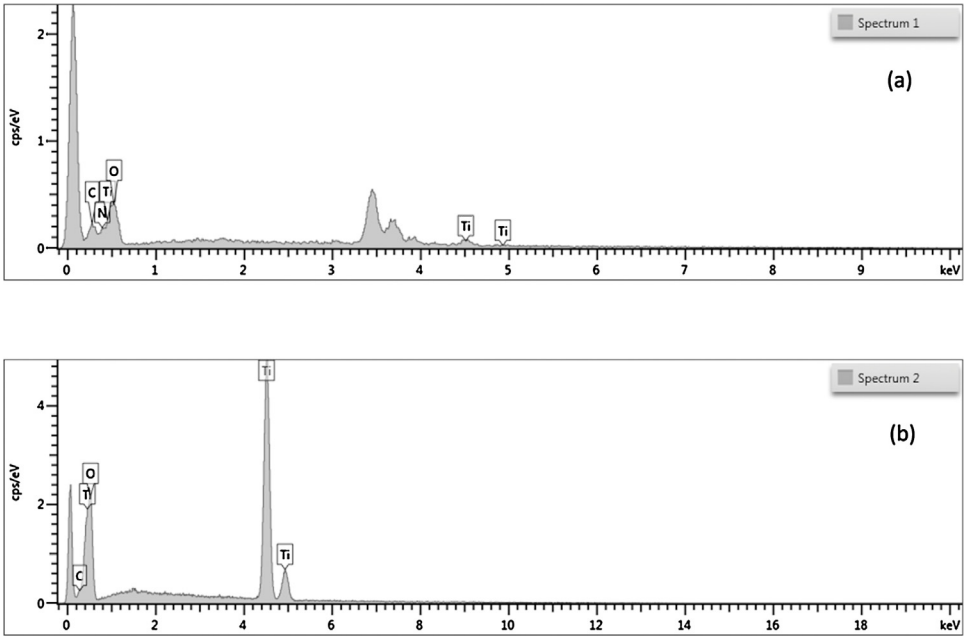

Fig. 2. EDX graphs of (a) Nitrogen doped TiO_2 electrode and (b) Normal TiO_2 electrode.

Table 1
EDX data (a) Nitrogen doped TiO_2 electrode and (b) TiO_2 electrode.

Element	Nitrogen doped TiO_2 electrode (atomic%)	Normal TiO_2 electr ode (atomic%)
Ti	20.33	51.71
O	55.03	44.47
N	5.12	0.00
C	19.52	3.82

Fig. 3. (a) Undoped TiO_2 powder in white colour (left) and (b) N-doped TiO_2 (right) powder in yellowish colour prepared in this work.

The XRD and XPS measurements on the N-doped TiO_2 (without graphine, Zr or Cu) in the above three systems reported by Kim et al. provide strong support to our findings for the N-doped TiO_2 material. That is, the Degussa P25 TiO_2 powder is composed of both anatase and rutile phases but the N-doped TiO_2 powder samples composed only of the anatase phase. Also, according to our XRD measurements, it is shown that the crystalline structure of TiO_2 did not changed due to N-doping which is also consistent with the findings reported by Kim et al. [30–32].

3.3. Optical absorption measurements analysis

The UV–vis absorption spectra derived from the diffused reflectance measurements (DRS) of undoped TiO_2 (curve, a) and N-doped TiO_2 powder samples (curve, b) are shown in Fig. 5(i). The nitrogen-doped titania powder has a deep yellow colour as shown in Fig. 3(b). It is evident from Fig. 3 the change in colour of the nanocrystals upon nitrogen incorporation demonstrates a profound effect on their optical response in the visible wavelength range (curve, b). The absorption spectrum of the nitrogen-doped titania powders exhibits a new characteristic absorption peak in the visible light region between 400 and 550 nm (curve, b) which cannot be seen in the spectrum obtained for the undoped TiO_2 powder (curve, a). This visible light absorption is considered to be due to the nitrogen doping in the TiO_2 crystalline structure. This is very likely due to a possibility of forming a new state close to the valence band edge of the TiO_2 induced by the nitrogen doping, as recently studied by Chen and Burda [29].

The band gaps of N-doped and undoped TiO_2 films were calculated from the following relationship.

$$\alpha = A(h\nu - E_g)^{1/2}/h\nu$$

where, α is the absorption coefficient, A is a constant, $h\nu$ is the energy of incident photon and E_g is the energy band gap. The plot of $(\alpha h\nu)^2$ versus $h\nu$ for the films are shown in Fig. 5(ii). According to Fig. 5(ii), the estimated values of band gap of undoped TiO_2 and N-doped TiO_2 were 3.28 eV and 3.13 eV respectively. It is clear that due to nitrogen doping the band gap of TiO_2 has been narrowed, thereby increasing the light harvesting.

According to the optical absorption measurements reported by Kim et al. [31,32] on TiO_2 incorporating Graphene/N, Zr/N and Cu/N, the absorption spectrum of the N-doped TiO_2 has shifted to an energy region lower than that of the pristine P25. In their work, most P25 nanoparticles had sizes ranging from 20 to 50 nm, whereas the N-doped TiO_2 nanoparticles had an average particle size of 30 nm. The average particle size of the Zr/Ndoped TiO_2 nanoparticles became smaller with increasing Zr content. The N

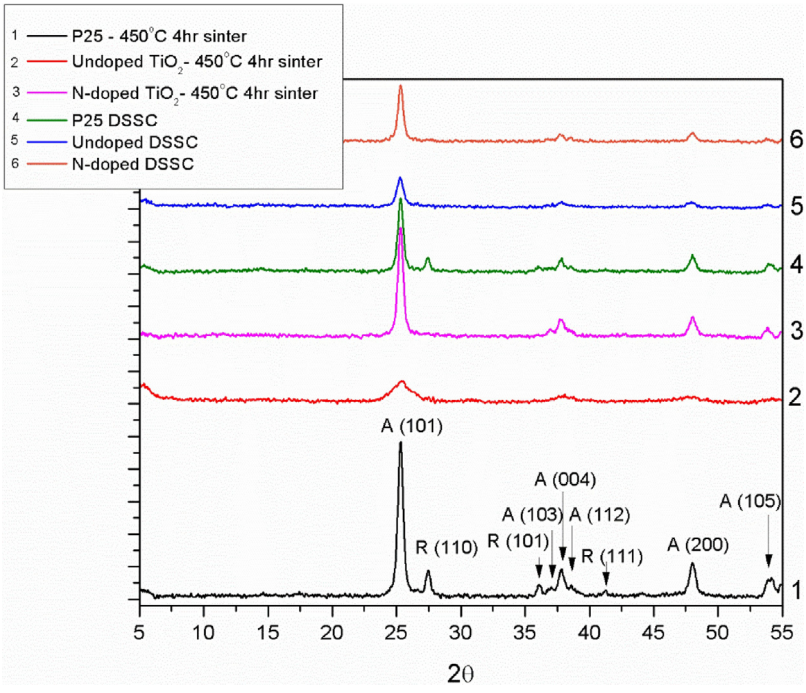

Fig. 4. The XRD patterns of the P25, undoped TiO_2 and N-doped TiO_2 powder samples.

Table 2
Phases of TiO_2 powder samples measured using XRD.

XRD sample	XRD Trace No. in Fig. 4	Anatase (%)
P25–450 °C 4hr sinter	1	80.7
Undoped TiO_2 – 450 °C 4hr sinter	2	100.0
N-doped TiO_2 – 450 °C 4hr sinter	3	100.0
P25 powder from DSSC	4	80.7
Undoped TiO_2 powder from DSSC	5	100.0
N-doped TiO_2 powder from DSSC	6	100.0

doping has lead to a red shift of the light absorption into the visible region, which has improved the light harvesting. The optical absorption spectrum of P25 revealed an absorption threshold at approximately 410 nm. The absorption spectrum of the N-doped TiO_2 (without Cu) was red shifted when compared to that of the P25. The addition of Cu has resulted in a further noticeable alteration of the spectra toward the visible-light region.

The results of the optical absorption measurements on N-doped TiO2 powder in our present work as described earlier are in good agreement with the results reported by Kim et al. for their N-doped TiO_2 powder s in all the three systems studied by them according to which, the optical absorption threshold has been red-shifted favouring increased visible light harvesting [30–32].

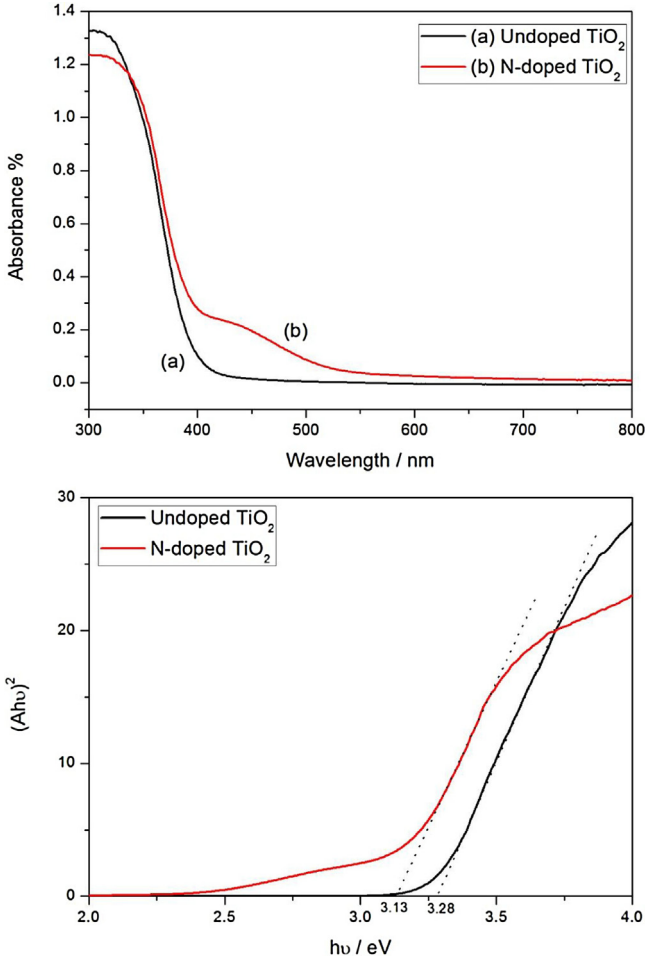

Fig. 5. (i) UV–vis optical absorption spectra derived from diffused reflectance of the (a) Undoped TiO_2 and (b) N-doped TiO_2 powders. (ii) Comparison of optical absorption curves for undoped and N-doped TiO_2 powders used for the determination of the energy band gap values.

3.4. Photovoltaic performance of DSSCs

DSSCs were fabricated using six different photoelectrode structures essentially with the same total thickness, as follows: Three single layer photoelectrode (A) P25 TiO_2, (B) undoped TiO_2 and (C) N-doped TiO_2 each with starting thickness ~9 μm and three multi-layer photoelectrode (D) compact layer/P25/P25, (E) compact layer/P25/undoped TiO_2 and (F) compact layer/P25/N-doped TiO_2, each with initial thickness ~19 μm and characterized by J-V measurements.

The current density- voltage (*J-V*) curves of DSSCs made with single layer and multiple layer photoelectrode are shown in Fig. 6. For these DSSCs, the fill factor (FF) is calculated using Eq. (1) and the overall energy conversion efficiency was calculated using Eq. (2).

$$FF = J_m V_m / J_{sc} V_{oc} \quad (1)$$

$$\eta = J_{sc} V_{oc} FF / \text{Total incident power density} \quad (2)$$

where V_m and J_m are the voltage and the current density respectively for the maximum power density output.

The short circuit photocurrent density J_{sc}, open-circuit photovoltage V_{oc}, the fill factor *FF*, and the efficiency η, derived from photo current density-voltage measurements of the six types of DSSCs are summarized in Table 3.

The DSSCs fabricated using photoelectrode with single layer, undoped and N-doped TiO_2 both achieved a lower energy conversion efficiency compared to DSSCs with single layer P25 photoelectrode. According to our observations, this low energy conversion efficiency was evidently due to the low short circuit current density (J_{SC}) values resulting from the poor adhesion of the undoped and N-doped TiO_2 particles to the FTO glass substrate. In order to overcome this difficulty and improve the adhesion between the TiO_2 powder and the FTO glass substrate, DSSCs with multi layered photoelectrode structures were prepared. Therefore, in order to overcome this problem here we introduced a new concept of multilayer structure by application of a compact layer and a P25 layer prior to depositing the undoped or N-doped layers, which essentially enhanced the overall performances of the DSSC as it is evident from Table 3.

As it is evident from Table 3, J_{SC} values and the overall efficiencies of the devices fabricated either with undoped (B) or N-doped (C) electrodes are lower than those obtained from the devices fabricated with P25 TiO_2. This might be due to the interfacial problems resulting from poor adhesion of the TiO_2 layers with the FTO substrate in the devices fabricated with only N-doped or undoped materials. Poor fill factor of cell (F) compared to cell (E) may be due to contact problems at interfaces. Both undoped and N-doped TiO_2 layers have poor adhesion onto FTO glass and onto P25 layer.

By introducing a compact layer and a P25 layer with a total thickness of ~9 μm in between the FTO glass and undoped or N-doped TiO_2 layer with the thickness of ~10 μm, the solar cell efficiencies for all three type DSSCs (C, D and F) were significantly increased. The conversion efficiency of the cells with N-doped TiO_2 was an impressive 8.00%, which is much higher than that of DSSCs with undoped TiO_2 (4.22%) and P25 (6.77%). The J_{SC} values followed a similar enhancement as the conversion efficiency. We believe that the increase of J_{SC} by 49% compared with undoped TiO_2 and 14% compared with P25 DSSC was a significant achievement in this work. The energy band narrowing in the N-doped TiO_2 materials appears to be primarily responsible for this photocurrent and efficiency enhancement, with some contribution from the increased dye absorption by the three-layer

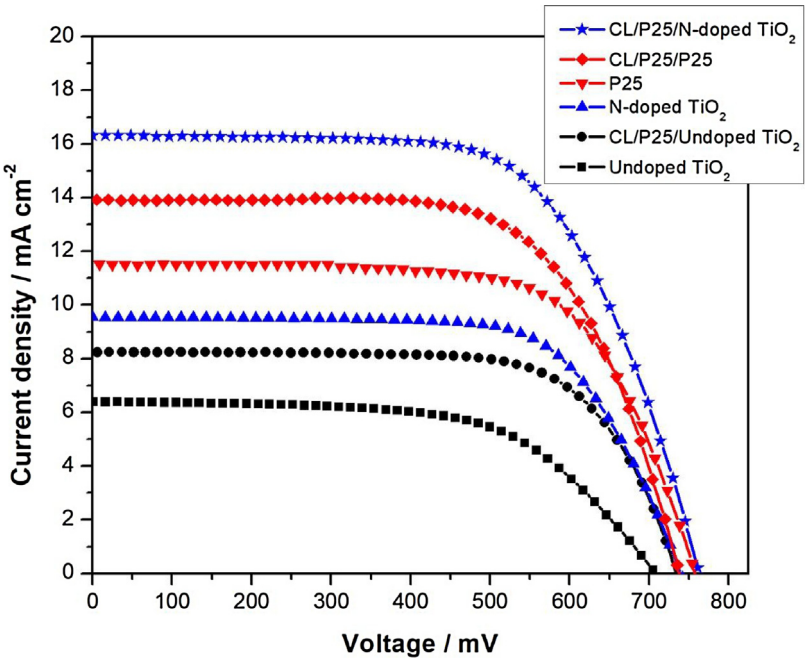

Fig. 6. Photocurrent density-voltage curves for DSSCs made with six different photoelectrode structures.

electrode configuration as evidenced from improved electron transport as discussed in the following sections.

3.5. IPCE spectra

In order to estimate the Quantum Efficiency which is a measure of how efficiently the device converts the incident light into electrical energy at a given wavelength the incident photon to current efficiency (IPCE) measurements were performed with the above all the devices in the wavelength range between 300 nm and 800 nm and results are shown in Fig. 7 and tabulated in Table 4.

As seen from Fig. 7, the highest IPCE is obtained for the DSSC fabricated with the configuration of compact layer/P25/N-doped TiO_2 multi-layer photoelectrode. A considerable difference in the IPCE maxima can be seen between the three layer electrodes with undoped and N-doped TiO_2 powders.

The IPCE peak height is maximum for the DSSC with compact layer/P25/N-doped TiO_2 photoelectrode (F) with a value of 67.02% at 535 nm. The improved performance of cells with N-doped TiO_2 electrode can be clearly seen in the IPCE spectra. These IPCE results are consistent with the photovoltaic parameters of the DSSCs shown in Table 3.

A significant enhancement of J_{SC} was achieved for the DSSCs with N-doped TiO_2 which has been confirmed by photocurrent-voltage measurement as well as by IPCE measurements. To find a relationship for the increase in J_{SC} values for the DSSCs with N-doped TiO_2 compared to those with undoped TiO_2, the amount of dye absorbance by the respective electrodes were estimated. The amounts of dye adsorbed by the three types of multilayer photoelectrodes (D, E and F) were measured using UV–visible spectrophotometer. The results revealed that the amount of dye adsorbed by the N-doped TiO_2 electrode (F) was the highest with a value of 2.43×10^{-7} mol cm^{-2}. The amount of dye adsorbed by the undoped TiO_2 electrode (E) was 2.27×10^{-7} mol cm^{-2} and by the P25 TiO_2 electrode (D) was 1.22×10^{-7} mol cm^{-2}. Tingli Ma and coworkers also reported that the amount of dye adsorbed by their N-doped TiO_2 electrode was higher compared to the P25 and undoped TiO_2 electrodes due to higher surface area and higher porosity of the N-doped powder [25]. They have confirmed these results by BET measurements. These results suggest that a contribution to enhancement of the short circuit current density J_{SC} and the conversion efficiency of the DSSCs comes from the increase in the amount of dye adsorbed by the N-doped TiO_2 electrodes possibly due to increased porosity. A major contribution for the intrinsic increase in th J_{SC} and IPCE, however, comes from the enhanced visible light absorption by the N-doped TiO_2 due to energy band gap narrowing as discussed earlier. This effect can clearly be seen in the broadened IPCE spectra of the DSSCs with N-doped TiO_2 electrodes in the wavelength range below 500 nm. This results suggests that the effect of energy band gap narrowing due to nitrogen doping is a more important fundamental intrinsic factor than the increased dye loading and can be effectively utilized in the development of photoelectrode for enhanced performance in DSSCs.

Table 3
Photovoltaic parameters of the DSSCs fabricated with single layer and multiple layer TiO_2 photoelectrodes.

Photoelectrode	J_{sc} (mA cm^{-2})	V_{oc} (mV)	FF%	ŋ %
(A) P25	11.50	755.9	67.9	5.90
(B) Undoped TiO_2	6.38	707.6	60.4	2.72
(C) N-doped TiO_2	9.52	742.6	68.54	4.84
(D) Compact layer/P25/P25	13.92	737.7	65.91	6.77
(E) Compact layer/P25/Undoped TiO_2	8.23	738.8	69.46	4.22
(F) Compact layer/P25/N-doped TiO_2	16.32	762.3	64.34	8.00

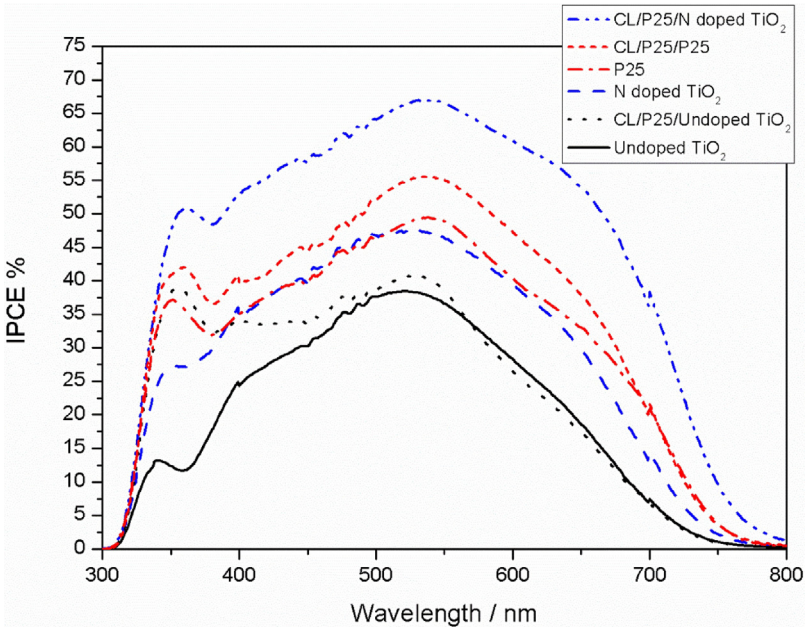

Fig. 7. The IPCE spectra for the DSSCs made with six different types of TiO_2 photoanodes given in Table 4.

Table 4
Peak wavelengths and peak hights (percentages) of the IPCE spectra of the six DSSC photoelectrodes.

DSSC photoelectrode configuration	IPCE peak wavelength (nm)	Peak percentage%
(A) P25	538	49.43
(B) Undoped TiO_2	523	38.40
(C) N-doped TiO_2	531	47.69
(D) Compact layer/P25/P25	533	55.50
(E) Compact layer/P25/Undoped TiO_2	527	40.76
(F) Compact layer/P25/N-doped TiO_2	535	67.02

3.6. Electrochemical impedance spectroscopic (EIS) analysis

In order to see the effect of N-doping in the electron transport of the N-doped TiO_2 based electrodes electrochemical impedance spectroscopy (EIS) measurements were carried out under the illumination of 100 mW cm^{-2} and obtained relevant Nyquist plots in order to study the internal resistances and the charge-transfer kinetics of the DSSCs. The charge transport properties of above six DSSCs extracted from the equivalent circuit analysis are listed in Table 5. In general, the EIS spectrum of liquid-electrolyte-based DSSCs exhibits three semi-circles, which are associated with the interfacial resistances and the oxidation-reduction reaction in DSSCs. These three interfacial resistances are related to the electrochemical reaction at the Pt/electrolyte interface ($R1_{CT}$), the charge-transfer process that occurs at the TiO_2/dye/electrolyte interface ($R2_{CT}$), and the Warburg diffusion of I_3^-/I^- in the electrolyte ($R3_{CT}$).

A Nyquist diagram of a DSSC typically features three semicircles in order of increasing frequency. These three semicircles correspond to the Nernst diffusion within the electrolyte, electron transport at the oxide/electrolyte interface and redox reaction at the platinum counter electrode. The impedance parameters were extracted using the equivalent circuits shown in the inset of Fig. 8 (a) and (b). The calculated values of the series resistance (R_s), charge-transfer resistance of the Pt/electrolyte interface ($R1_{CT}$), charge transfer resistance of the TiO_2/electrolyte interface ($R2_{CT}$) and ion diffusion of the electrolyte ($R3_{CT}$) based on the equivalent circuit analysis of the six types of DSSCs are shown in Table 5 [33].

As seen from Table 5, the charge transfer resistance of the TiO_2/electrolyte interface ($R2_{CT}$) value of the N-doped TiO_2 based DSSCs is lower than the P25 and undoped TiO_2 based DSSCs. This may due to the change in the surface properties of the TiO_2 film due to nitrogen doping. The Table 5 further shows that the J_{SC} values of the DSSCs with electrodes D, E and F have increased with decreasing

Table 5
Series resistance (R_s), charge transfer resistance of the Pt/electrolyte ($R1_{CT}$), charge transfer resistance of the TiO_2/electrolyte ($R2_{CT}$) and charge transfer resistance of the TiO_2/FTO ($R3_{CT}$) of DSSCs with single layer and multi-layer TiO_2 photoelectrodes.

Type of photoelectrode	J_{sc} (mA cm^{-2})	Eff%	R_s (Ω)	$R1_{CT}$ (Ω)	$R2_{CT}$ (Ω)	$R3_{CT}$ (Ω)
(A) P25	11.50	5.90	13.60	11.80	11.80	3.51
(B) Undoped TiO_2	6.38	2.72	15.00	6.95	11.40	55.70
(C) N-doped TiO_2	9.52	4.84	12.60	2.64	1.31	47.30
(D) Compact layer/P25/P25	13.92	6.77	28.30	7.71	5.56	17.50
(E) Compact layer/P25/Undoped TiO_2	8.23	4.22	24.20	18.00	8.02	18.50
(F) Compact layer/P25/N-doped TiO_2	16.32	8.00	16.10	7.66	5.43	17.10

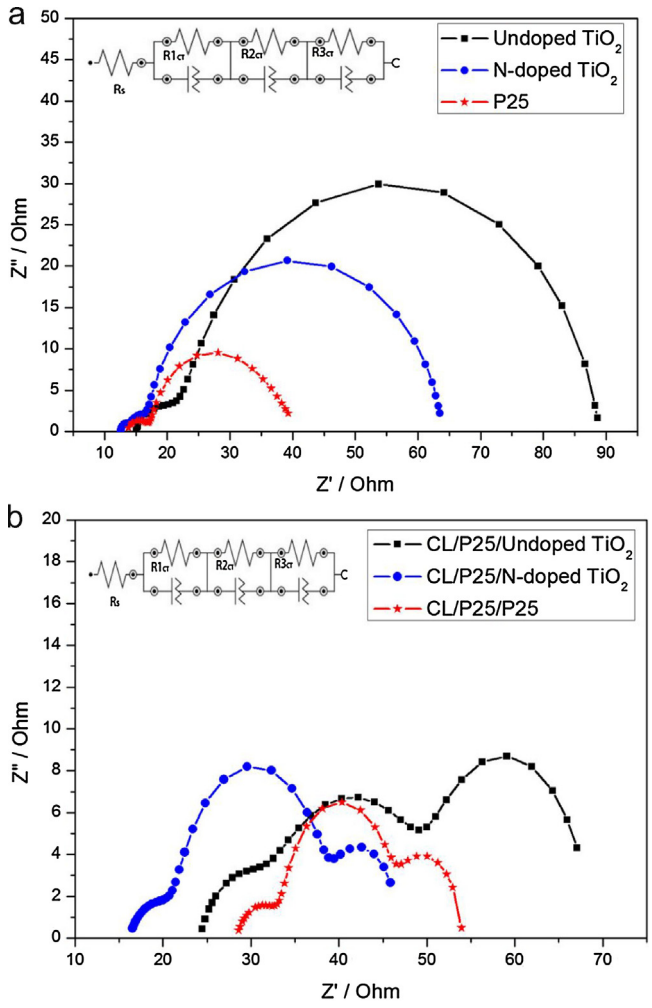

Fig. 8. (a). Impedance plots taken for the three different DSSCs with single layer photoelectrodes: (A) P25, (B) undoped TiO_2 and (C) N-doped TiO_2. (b). Impedance plots taken for the three different DSSCs with multilayer photoelectrodes: (D) CL/P25/P25, (E) CL/P25/undoped TiO_2 and (F) CL/P25/N-doped TiO_2.

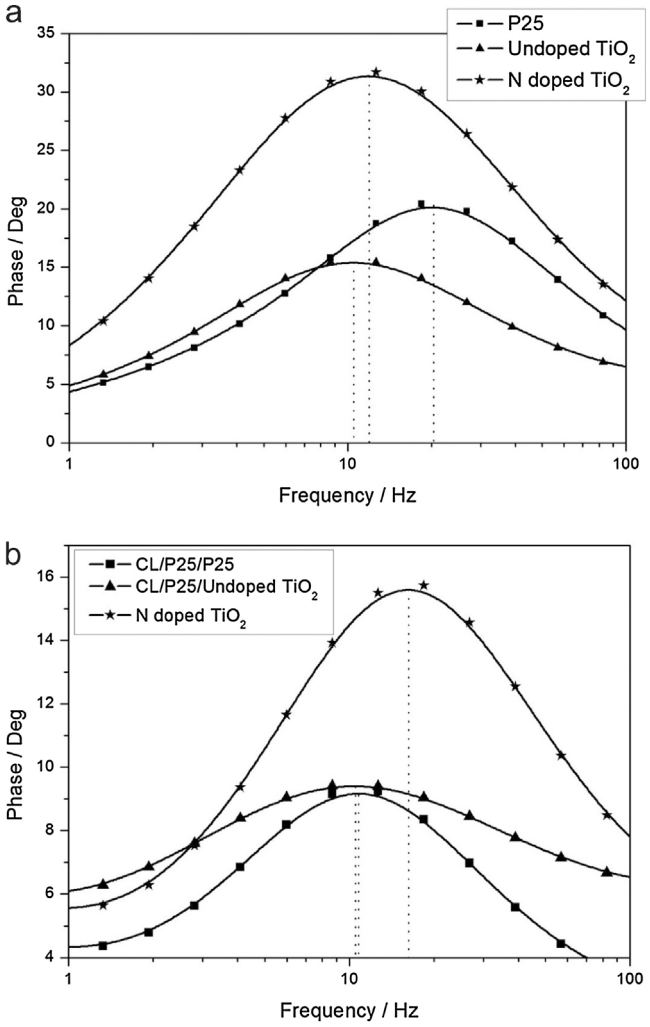

Fig. 9. (a). Bode plots for the three DSSCs with (A) P25, (B) undoped TiO_2 and (C) N-doped TiO_2. single layer electrodes in the frequency range of 1×10^{-2}–1×106 Hz. (b). Bode plots for the three DSSCs with (D) CL/P25/P25, (E) CL/P25/undoped TiO_2 and (F) CL/P25/N-doped TiO_2 multiple layer electrodes in the frequency range of 1×10^{-2}–1×10^{6} Hz.

$R2_{CT}$ value in the order CL/P25/Undoped TiO_2, CL/P25/P25 and CL/P25/N-TiO_2. The lower $R2_{CT}$ value in the N-doped TiO_2 based DSSC implies that the electron transfer mechanism at the TiO_2/electrolyte interface has improved due to nitrogen doping.

Cell E shows low current density than cell A. Charge transfer resistance of the TiO_2/FTO interface ($R3_{CT}$) of Cell A is lower than that of the Cell E. From this, it can be concluded that the adhesion and contacts between TiO_2 and FTO is better in cell A.

N-doped TiO_2 photoelectrode have improved electron transport property. This has been studied by Wei Guo et al. using intensity-modulated photocurrent and photovoltage spectroscopy (IMPS) [34]. $R2_{CT}$ value decreases with increasing electron transport property. Cell (D), (E) and (F) have multilayers and $R2_{CT}$ gives as net resistance of TiO_2/electrolyte interface. Therefore, $R2_{CT}$ value of single layered N-doped TiO_2 DSSC (cell C) is lower than other cells which have more interfaces due to multilayered nature of these electrodes.

Bode phase plots derived from EIS measurements on DSSCs are shown in Fig. 9(a) for the P25, undoped TiO_2 and N-doped TiO_2 (A, B and C) electrodes and in Fig. 9(b) for the multilayer, D, E and F electrodes. The electron life time (τ_e) can be estimated by $\tau_e = 1/(2\pi f_{max})$ where f_{max} is the frequency correspond to the peak in the Bode phase value [18]. From Fig. 9(a) and (b), it can be seen that the electron lifetime of the DSSC with N-doped TiO_2 were lower than the solar cell with undoped TiO_2. Also it can be seen that the electron lifetime decreases with increasing efficiency of DSSCs. Table 6 shows the maximum frequency value (f_{max}) and the electron life time (τ_e) for each DSSC configuration. It should be noted that as seen from Table 6, the electron lifetime of N-doped TiO_2 (13.29 ms) is higher than the value for P25 (7.80 ms). Similar enhancement of lifetime compared to P25 has been reported by T. K. Yun et al. [27].

According to Table 6, the electron lifetime (τ_e) value is lower in the DSSCs with CL/P25/N-doped TiO_2 electrode compared to the DSSCs with CL/P25/Undoped TiO_2 electrode. Normally electron lifetime should increase with the enhancement of efficiency.

Table 6
Electron life times (τ_e) extracted from the Bode plots shown in Fig. 9(a) and (b).

TiO_2 electrode configuration	Efficiency	f_{max}/Hz	τ_e/ms
(A) P25	5.90	20.41	7.80
(B) Undoped TiO_2	2.72	10.49	15.17
(C) N-doped TiO_2	4.84	11.97	13.29
(D) Compact layer/P25/P25	6.77	10.77	14.77
(E) Compact layer/P25/Undoped TiO_2	4.22	10.51	15.14
(F) Compact layer/P25/N-doped TiO_2	8.00	16.26	9.78

However, due to other conditions, such as increased recombination and thickness of the photoanode electron lifetime may decrease for high efficiency DSSCs. In the present example, DSSC with N-doped TiO_2 electrodes possess higher photocurrent due to increased light harvesting by modified energy band gap and also due to higher dye uptake as described earlier. These effects are evidently more dominant and surpass the negative effect due to reduced lifetime and faster recombination. In other words, electron lifetimes and recombination effect alone cannot determine the net solar cell efficiency [35].

4. Conclusion

Nitrogen doped TiO_2 powder was prepared and characterized. Energy band gap narrowing due to N-doping has been established. A series of single layered and multi layered photoanode structures for DSSCs consisting of P25 TiO_2, undoped TiO_2 and N-doped TiO_2 were prepared. The best energy conversion efficiency of 8% was achieved for the DSSCs with Compact Layer/P25/N-doped TiO_2 three layer electrodes, which was about 89% higher than the DSSCs with Compact Layer/P25/Undoped TiO_2 three layer electrodes. Moreover, DSSCs with the three layer electrode incorporating the N-doped TiO_2 possess higher photocurrent due to increased light harvesting by modified energy band gap and due to higher dye uptake. Also, an enhanced open circuit photovoltage and faster electron transport by low charge transfer resistance were obtained for the DSSCs with N-doped TiO_2 electrodes. All these favourable factors associated with N-doped TiO_2 electrodes contributed significantly to the enhanced photovoltaic performance of DSSCs. However, the shorter electron lifetime giving higher electron recombination in the N-doped electrode works towards lowering the DSSC performance but this effect appears to be less dominant.

References

[1] B. O'Regan, M. Grätzel, A low-cost, high-efficiency solar cell based on dye-sensitized colloidal TiO_2 films, Nature 353 (1991) 737–740.
[2] K. Hara, H. Arakawa, Handbook of Photovoltaic Science and Engineering, (2003) 0-471-49196-9 (664).
[3] N. Koumura, Z. Wang, S. Mori, M. Miyashita, E. Suzuki, K. Hara, Alkyl-functionalized organic dyes for efficient molecular photovoltaics, J. Am. Chem. Soc. 128 (2006) 14256–14257.
[4] M. Grätzel, Solar energy conversion by dye-sensitized photovoltaic cells, Inorg. Chem. 44 (2005) 6841–6851.
[5] M.A.K.L. Dissanayake, C.A. Thotawatthage, G.K.R. Senadeera, T.M.W.J. Bandara, W.J.M.J.S.R. Jayasundera, B.-E. Mellander, Efficiency enhancement by mixed cation effect in dye-sensitized solar cells with PAN based gel polymer electrolyteJ, Photochem. Photobio. A 246 (2012) 29–35.
[6] H. Wang, X. Zhang, F. Gong, G. Zhou, Z. Wang, Novel ester-Functionalized solid-state electrolyte for highly efficient all-solid-state dye-sensitized solar cells, Adv. Mater. 24 (2012) 121–124.
[7] H. Zheng, Y. Tachibana, K. Kalantar-zadeh, Dye-Sensitized solar cells based on WO_3, Langmuir 26 (2010) 19148–19152.
[8] S. Yang, H. Kou, J. Wang, Tunability of the band energetics of nanostructured $SrTiO_3$ electrodes for dye-Sensitized solar cells, J. Phys. Chem. C 114 (2010) 4245–4249.
[9] K. Rokesh, A. Pandikumar, K. Jothivenkatachalam, Dye sensitized solar cell: a summary, Mater. Sci. Forum 771 (2014) 1–24.
[10] Q. Zhang, T.P. Chou, B. Russo, Aggregation of ZnO nanocrystallites for high conversion efficiency in dye-sensitized solar cells, Angew. Chem. Int. Ed. 47 (2008) 2402–2406.
[11] J.F. Qian, P. Liu, Y. Xiao, TiO_2-Coated multilayered SnO_2 hollow microspheres for dye-sensitized solar cells, Adv. Mater 21 (2009) 3663–3667.
[12] K. Sayama, H. Sugihara, H. Arakawa, Photoelectrochemical properties of a porous Nb_2O_5 electrode sensitized by a ruthenium dye, Chem. Mater. 10 (1998) 3825–3832.
[13] K.-P. Wang, H. Teng, Zinc-doping in TiO_2 films to enhance electron transport in dye-sensitized solar cells under low-intensity illumination, Phys. Chem. Chem. Phys. 11 (2009) 9489–9496.
[14] X. Lu, X. Mou, J. Wu, Improved-performance dye-sensitized solar cells using Nb-doped TiO_2 electrodes: efficient electron injection and transfer, Adv. Func. Mater. 20 (2010) 509–515.
[15] M.A.K.L. Dissanayake, J.M.K.W. Kumari, G.K.R. Senadeera, C.A. Thotawatthage, Efficiency enhancement in plasmonic dye-sensitized solar cells with TiO_2 photoanodes incorporating gold and silver nanoparticles, J. App. Elec. 46 (2016) 47–58.
[16] A. Pandikumar, S.P. Lim, S. Jayabal, N.M. Huang, H.N. Lim, R. Ramaraj, Titania@gold plasmonic nanoarchitectures: an ideal photoanode for dye-sensitized solar cells, Renew. Sustain. Energy Rev. 60 (2016) 408–420.
[17] R. Asahi, T. Morikawa, T. Ohwaki, Visible-light photocatalysis in nitrogen-doped titanium oxides, Science 293 (2001) 269–271.
[18] H.J. Tian, L.H. Hu, C.N. Zhang, S.H. Chen, J.A. Sheng, L. Mo, W. Liu, S. Dai, Enhanced photovoltaic performance of dye-sensitized solar cells using a highly crystallized mesoporous TiO_2 electrode modified by boron doping, J. Mater. Chem. 21 (2011) 863–868.
[19] D. Chu, X. Yuan, G. Qin, M. Xu, P. Zheng, Efficient carbon-doped nanostructured TiO_2 (anatase) film for photoelectrochemical solar cells, J. Nanopart. Res. 10 (2008) 357–363.
[20] A. Yella, H.W. Lee, H.N. Tsao, C. Yi, C.A. Kumar, M.K. Nazeeruddin, E.G. Diau, C.Y. Yeh, S.M. Zakeeruddin, M. Gratzel, Prophyrin-sensitized solar cells with cobalt based redox electrolyte exceed 12 percent efficiency, Science 334 (2011) 629–634.
[21] W. Guo, Y. Shen, L. Wu, Y. Gao, T. Ma, Effect of n dopant amount on the performance of dye-sensitized solar cells based on N-Doped TiO_2 electrodes, J. Phys. Chem. C 115 (2011) 21494–21499.
[22] T. Ma, M. Akiyama, E. Abe, I. Imai, High-Efficiency dye-Sensitized solar cell based on a nitrogen-doped nanostructured titania electrode, Nano Lett. 5 (2005) 2543–2547.
[23] S. Livaraghi, M.C. Paganini, E. Giamello, Origin of photoactivity of nitrogen-doped titanium dioxide under visible light, J. Am. Chem. Soc. 128 (2006) 15666–15671.
[24] C.R. Torres, T. Lindgren, J. Lu, C.-G. Granqvist, S.-E. Lindqvist, Photoelectrochemical study of nitrogen-doped titanium dioxide for water oxidation, J. Phys. Chem. B 108 (2004) 5995–6003.
[25] S. Sato, R. Nakamura, S. Abe, Visible-light sensitization of TiO2 photocatalysts by wet-method N doping, Appl. Cata. A: General 284 (2005) 131–137.
[26] Y.Q. Wang, X.J. Yu, D.Z. Sun, Synthesis characterization, and photocatalytic activity of TiO2-xNx nanocatalyst, J. Hazar. Mater. 144 (2007) 328–333.
[27] T.K. Yun, J.H. Cheon, J.Y. Bae, K.S. Ahn, J.H. Kim, Enhanced electron lifetime on nitrogen-doped TiO_2 films for dye-sensitized solar cells, J. Nanosci & Nanotech. 12 (2012) 3305–3308.
[28] X. Qiu, C. Burda, Chemically synthesized nitrogen-doped metal oxide nanoparticles, Chem. Phys. 339 (13) (2007) 1–10.
[29] Xiaobo Chen, Clemens Burda, The electronic origin of the visible-light absorption properties of C-, N- and S-Doped TiO_2 nanomaterials, J. Am. Chem. Soc. 130 (15) (2008) 5018–5019.
[30] Seong-Bum Kim, Jun-Yong Park, Chan Soo Kim, Kikuo Okuyama, Sung-Eun Lee, Hee Dong Jang, Tae Oh Kim, Effects of graphene in dye-sensitized solar cells based on nitrogen- doped TiO_2 composite, J. Phys. Chem. C 119 (29) (2015) 16552–16559.
[31] Jun-Yong Park, Kyu-Han Lee, Beom-Soo Kim, Chan-Soo Kim, Sung-Eun Lee, Kikuo Okuyama, Hee-Dong Jan, Tae-Oh Kim, Enhancement of dye-sensitized solar cells using Zr/N-doped TiO2 composites as photoelectrodes, RSC Adv. 4 (2014) 9946–9952.
[32] Jun-Yong Park, Chan-Soo Kim, Kikuo Okuyama, Hye-Moon Lee, Hee-Dong Jang, Sung-Eun Lee, Tae-Oh Kim Copper and nitrogen doping on TiO_2 photoelectrodes and their functions in dye-sensitized solar cells, J. Power Sources 306 (2016) 764–771.
[33] T. Hoshikawa, T. Ikebe, R. Kikuchi, K. Eguchi, Effects of electrolyte in dye-sensitized solar cells and evaluation by impedance spectroscopy, Electrochim. Acta 51 (2006) 5286–5294.
[34] W. Guo, L. Wu, Z. Chen, G. Boschloo, A. Hagfeldt, T. Ma, Highly efficient dye-sensitized solar cells based on nitrogen-doped titania with excellent stability, Photochem. Photobiol. A: Chem. 219 (2011) 180–187.
[35] K. Kalyanasundaram, Dye-Sensitized Solar Cells, 1st edition, EPFL press, 2010 (95).